https://doi.org/10.5194/essd-2022-71
Preprint. Discussion started: 11 March 2022

Open Access Earth System Science Data Discussions

A new estimate of oceanic CO_2 fluxes by machine learning reveals the impact of CO_2 trends in different methods

Jiye Zeng[1], Tsuneo Matsunaga[1], and Tomoko Shirai[1]

[1]National Institute for Environmental Studies, Tsukuba, 305-8506, Japan

Correspondence to: Jiye Zeng (zeng@nies.go.jp)

Abstract. Global oceans have absorbed a substantial portion of the anthropogenic carbon dioxide (CO_2) emitted into the atmosphere. Data-based machine learning (DML) estimates for the oceanic CO_2 sink have become an import part of the Global Carbon Budget in recent years. Although DML models are considered objective as they impose very few subjective conditions in optimizing model parameters, they face the challenge of data scarcity problem when applied to mapping ocean CO_2 concentrations, from which air-sea CO_2 fluxes can be computed. Data scarcity forces DML models to pool multiple years' data for model training. When the time span extends to a few decades, the result could be largely affected by how ocean CO_2 trends are obtained. This study extracted the trends using a new method and reconstructed monthly surface ocean CO_2 concentrations and air-sea fluxes in 1980-2020 with a spatial resolution of 1x1 degree. Comparing with six other products, our results show a smaller oceanic sink and the sink in early and late year of the modelled period could be overestimated if ocean CO_2 trends were not well processed by models. We estimated that the oceanic sink has increased from 1.79±0.47 PgC yr^{-1} in 1980s to 2.58±0.20 PgC yr^{-1} in 2010s with a mean acceleration of 0.027 PgC yr^{-2}.

1 Introduction

The carbon dioxide (CO_2) emitted into the atmosphere by human activities has been considered a key factor causing abnormal climate changes for decades and the oceans play a crucial role in mitigating against the increase of atmospheric CO_2 (Sabine et al., 2004; Khatiwala et al., 2013; McKinley et al., 2016). The Global Carbon Budget 2021 (Friedlingstein et al., 2021) derived the oceanic sink from the average of flux estimates by biogeochemistry models and by data-based machine learning (DML) models. Although DML models are more objective in terms of optimization as they do not impose subjective conditions on the valid ranges of model parameters, under learning or overfitting due to data scarcity could result in false extrapolations to unsampled domains. Reconstructing surface ocean CO_2 (simply refer to as ocean CO_2 or simply CO_2 thereafter) by DML models for flux estimate also faces the same challenge.

The Surface Ocean CO_2 Atlas (SOCAT) Database Version 2021 (Sabine et al., 2013; Pfeil et al., 2013; Bakker et al.,2016) is a combined product of in situ measurements of ocean CO_2 by internationally coordinated efforts. It shows a composite sampling map covering most areas of the oceans. However, only a small portion of the oceans had samples in any single year

https://doi.org/10.5194/essd-2022-71
Preprint. Discussion started: 11 March 2022

and the sampling is extremely unbalance in season and geography (refer to Supplement 1). This situation forced DML models to pool multiple years data for training. The dilemma is while ocean CO_2 tends to track the increase in atmospheric CO_2 closely (Fay and McKinley, 2013; Bates et al., 2014), the large seasonal and special viabilities of CO_2 up to a few hundred μatm makes it difficult to detect its annual increase rate in the order of a few μatm per year. Current methods for solving the problem include normalizing ocean CO_2 to a reference year (Takahashi et al. 2009; Sasse et al., 2012 & 2013; Nakaoka et al., 2013; Zeng et al., 2014), including a linear time-dependent term in regression (Fay and McKinley, 2013; Iida et al., 2015, 2021; Jones et al., 2015; Watson et al., 2020), and using atmospheric CO_2 as a predictor to make DML models learn the trend implicitly (Landschützer et al., 2016; Gregor and Gruber, 2021; Denvil-Sommer et al., 2019; Chau et al., 2021). The former two methods assume a constant trend for the whole model period. It could be a good approximation when the time span is short but tends to overestimate the annual increase rate of CO_2 in early years and underestimate the rate in later years with the time extended to a few decades. As for the third approach, Landschützer et al. (2016) has shown that if several years of observations were withheld from the training at the beginning or the end, then the trend is ill constrained during these years, leading to larger errors. The evaluation of Gloege et al. (2021) also shows that the method was less capable in reconstructing variability at decadal timescales.

There are two camps of DML models in ocean CO_2 reconstruction in terms of data pooling strategy. One camp treated the global oceans as one entity (Takahashi et al., 2009; Sasse et al., 2013; Nakaoka et al., 2013; Zeng et al., 2014; Denvil-Sommer et al., 2019; Chau et al., 2021). Methods in this camp sacrifices the accuracy of region-dependent trends to ease the scarcity problem. An apparent global trend was thus derived and used. Another camp divided the oceans into clusters with similar biogeochemical properties. Sasse et al. (2012, 2013) and Landschützer et al. (2013,2016) are early pioneers in this camp. They used Self-Organization Map (SOM) for clustering in the first step and then used different regression methods in the second step for making prediction. The two-step method of Landschützer et al. (2016) was also used by Laruelle et al. (2017), Watson et al., 2020, and Gloege et al. (2021). Other clustering methods include geographical blocking (Iida et al., 2015; Watson et al., 2020), K-mean clustering (Gregor et al., 2019; Gregor and Gruber, 2021), and CO_2 biome clustering (McKinley et al., 2011; Fay and McKinley, 2013; Gregor et al., 2019; Watson et al., 2020). Post smoothing is necessary for clustering methods to make the spatial changes of CO_2 contingent. An advantage of the two-step method is that the clustering brings together regions with similar seasonality and similar co-variability with predictors. While this approach could partially reduce factors that obstruct the extraction of ocean CO_2 trend, the data scarcity problem tends to become more severe in some clusters.

This study used three DML models to extend the work of Zeng et al. (2014) by using a new method to extract ocean CO_2 trends in decadal scales. It largely reduced the error of using a constant trend to reconstruct ocean CO2 that resulted in overestimates of CO_2 uptake in the starting and ending years. Our models yielded smaller air-sea CO_2 fluxes comparing to six other products included in Global Carbon Budget 2021 (Friedlingstein et al., 2021).

https://doi.org/10.5194/essd-2022-71
Preprint. Discussion started: 11 March 2022

2 Method

2.1 Model Setup

Following Zeng et al. (2014, 2017), we express the nonlinear dependence of ocean CO_2 on time and biogeochemical variables as

$$CO2W = f(SST, dSST, SSS, CHL, MLD, LAT, LON) + f(year) \quad (1)$$

where SST stands for sea surface temperature, SSS for sea surface salinity, CHA for chlorophyll-a concentration, MLD for mixed layer depth, LAT for latitude and LON for longitude. The sine and cosine converted values of LON were used to make the circular variable contingent. We replaced the month variable of Zeng et al. (2014) with SST anomaly (dSST) against the annual mean to harmonize the seasons of the two hemispheres. The function of year represents the increase rate of CO_2, which was a constant in Zeng et al. (2014). We deployed three databased machine learning (DML) methods to model the rate: Random Forest (RF), Gradient Boost Machine (GBM), and Feedforward Neural Network (FNN). Using multiple models has the merit points that we can check overfitting better and compensate their weakness with each other.

RF was proved to be a robust method for modelling carbon flux at global scale (Zeng et al., 2020) and was applied to global ocean CO_2 mapping recently (Gregor et al., 2019). We used the python library of Ranger (Weight & Ziegler, 2017) that implements the regression algorithm using two-stage randomization procedure to partition trees. A tree is assigned a subset of the training data randomly sampled with repetition; then it is recursively split into binary nodes until the number of data points in terminal nodes becomes no larger than a specified number. In each split, the RF randomly selects a subset of predictor variables and searches them for splitting points that minimize node impurity (Ishwaran, 2015). In making a prediction, a set of predictors are passed through branches of nodes according to the splitting rule until the journey ends up in a terminal node. The mean of the target variable in the terminal node is taken as an estimate. Then the average estimate of all terminal nodes is used as the prediction. One can see that predictions are confined in the range of observations. Sensitive factors for configuring the RF include the number of trees and the number of data points in terminal nodes (Zeng et al., 2020). The default setting includes 500 trees and 5 data points. We raised the data points to 100 based on out experiments with ocean CO_2 data. The configuration yielded good validation results.

GBM is also a decision-tree based machine learning model and emerged in the ocean CO_2 mapping recently (Gregor et al., 2019; Gregor and Gruber, 2021). Like RF, GBM combines weak learners into a single strong learner (Natekin and Knoll, 2013), but in an iterative fashion. Trees are added one at a time, and existing trees in the model are not changed. The gradient descent procedure is used to optimize parameters of new trees to reduce the loss of predictions made with old trees. As the tree parameters are used in making predictions, the target could be extrapolated beyond the range of observations. We used the python library of LightGBM (Ke et al., 2017). By experimenting with ocean CO_2 data and using the RF as a reference, we

https://doi.org/10.5194/essd-2022-71
Preprint. Discussion started: 11 March 2022

found that LightGBM performs well with 500 trees, minimum of 100 terminal nodes in a tree, and 100 data points in a terminal node.

FNN has been used for ocean CO2 mapping since early 2010s (e.g., Landschützer et al., 2013; Zeng et al., 2014). FNN has a layered structure, including an input layer, one or more hidden layers, and an output layer. Neurons between adjacent layers are fully connected. Details of FNN can be found in Svozil et al. (1997) and abundant of other references. We used python's MLPRegressor with one hidden layer and 256 hidden neurons. The early stop of training iteration was set to 300. From experiments with the ocean CO_2 data, we found that the FNN was sensitive to those parameters when LAT and LON were included as predictors. The configuration yielded results well harmonized with those of the RF and GBM. In contrast to the RF and GBM, observations of the target variable are not used for making predictions. While this benefits data mining for making new discoveries, overfitting and extrapolation are more likely to emerge.

2.2 Data

We extracted monthly CO_2 fugacity (fCO_2) from the track-gridded database of the Surface Ocean CO_2 Atlas (SOCAT) version 2021 (Sabine et al., 2013; Pfeil et al., 2013; Bakker et al., 2016). We relaxed the criteria of Zeng et al. (2014) for data selection: (i) fCO_2 values smaller than 700 μatm and larger than 100 μatm and (ii) salinity larger than 15.0. A total of 273,434 data points were extracted from 1x1 degree grids for 1980-2020. We confine fCO_2 training data set to be post-1980 due to large uncertainties in early measuring techniques (Sasse et al., 2013). The sources of predictor variables are shown in Table 1. The values of CHL and MDL were scaled by log(1+CHL) and log(1+MDL) to reduce the skewness of sample distribution. We used the monthly surface air pressure (Ps) of the fifth generation ECMWF atmospheric reanalysis of the global climate (ERA5) to convert reconstructed fCO_2 to partial pressure for flux calculation. The partial pressure of air CO_2 (pCO2A) came from NOAA's Marine Boundary Layer Reference (Conway et al., 1994; Dlugokencky et al., 2019) and the monthly wind speed (WIND) from ERA5.

For training models, raw ocean CO_2 data were normalized to the reference year 2000 by

$$CO2W^{norm}(year) = CO2W^{raw}(year) - \sum_{i=2000}^{year} sign(i-2000)\cdot rate(year). \quad (2)$$

CO_2 concentrations were reconstructed by adding the rate correction of Eq.2 to the predicted CO_2. The fugacity was converted to partial pressure by the method of Weiss (1974). CO_2 fluxes were calculated by the difference of CO_2 partial pressures between air (pCO2A) and sea (pCO2W):

$$flux = k_w k_0 (pCO2W - pCO2A), \quad (3)$$

where k_w is the gas transfer velocity, and k_0 the solubility of CO_2 in seawater. The two parameters were obtained based on Wanninkhof (2014).

https://doi.org/10.5194/essd-2022-71
Preprint. Discussion started: 11 March 2022

2.3 Rate Extraction

We used iteration method of Zeng et al. (2014) with variable length of data to estimate the annual increate rate of ocean CO_2 at decadal scale. The method fits the dependence of CO_2 on year (the second term in Eq.1) by linear regression, subtracts the trend from observations, and then used the RF, GBM, and FNN to model the nonlinear relationship between the residual and predictors (the first term in Eq.1). The shortest data length is three years: data of the target year plus one year before and after the year. The longest data length is 41 years for the target year 2000, i.e., all data in 1980-2020 were included. These results provide valuable information on how to determine the annual rates.

3. Results

3.1 Annual Rate

The annual increase rates of ocean CO_2 obtained using the iteration method and the longest available data are shown in Fig. 1a along with the global annual increase rates of air CO_2 from the Global Monitoring Laboratory of NOAA (Conway et al., 1994) and the moving average of the rate with window size of 11 years (5 years before and after a given year). Ideally the rate for a target year should be extracted with the shortest data length possible. Because of data scarcity and the complexity of CO_2 dependence on time and the biogeochemical properties of seawaters, the rates fluctuate dramatically when data length is short and converges with increasing data length (Fig. 1b-d). Sutton et al. (2019) concluded that the number of years of observations needed (YON) to detect a statistically significant trend over variability range from 8 to 15 years at several open ocean sites. It is reasonable to assume that YON for open oceans would not be smaller. Because it is difficult to determine the smallest stabilization length, and the rates do not change much after 10 to 15 years, we used the rates with the maximum data length. As a result, the rate for 2000 (1.71 μatm yr^{-1}) is equivalent to the long-term trend of 1980-2020.

The rates appear to track the monotonical increase of the decadal mean rates of air CO_2 in 1997-2015 and remain flat with small changes in 1990-1996 during which air CO_2 rates experienced a long period of decline. Fig. 1b-d reveal that it requires at least 7 years' observations to detect the trend at the global scale. Comparing to a fixed site, the spatial variability imposes an additional interference to trend detection. The YON was about 20 years in early 1990s (Fig. 1b) when samples were few and incomplete in season (Supplement Fig. 1) and about 9 years in early 2010s (Fig. 1d) when samples were relatively abundant. Around year 2000, the trend became rather stable when the data length exceeds 10 years (Fig. 1c) but continued to go up and down with data length. One of the reasons must be that the data points after 2000 overwhelm data before the year. With the extension of data length, the trend tends to be affected more and more by data in later years.

The orange line in Fig. 1a represents the annual rates for data normalization in this study. We assumed that the rates before 1990 is the same as in 1990, i.e., 1.46 μatm yr^{-1}. This value is close to the rate of 1.50 μatm yr^{-1} used by Takahashi et al. (2009)

https://doi.org/10.5194/essd-2022-71
Preprint. Discussion started: 11 March 2022

and Zeng et al. (2014), and to the mean decadal trend of air CO_2 (1.49 ppm yr^{-1}) in the same period. Further, we assume that the rate ratio between ocean and air CO_2 after 2015 is the same as that in 2015 (0.941) and used the ratio to calculate the annual rate of ocean CO_2 in 2016-2020.

3.2 Model Performance

We used a so-called leave-one-year-out (LOYO) method to validate model performance. Giving N years of data, N validations were done by setting aside one year's data for validation and using other N-1 years of data for training. A model's performance was evaluated by biases in all validation years. The method has an advantage over the conventional n-fold validation method in that the validation data of LOYO are more likely come from unsampled domains of the training data.

As a test for the method itself, we used it with raw CO_2 data to investigate the long-term trend. In the first round, the residue of prediction minus observation shows a significant (R^2=0.971) negative correlation with time (Supplement Fig. 2a). This is expected as the CO_2 concentrations in early years tend to be overestimated by the models trained with increased CO_2 in later years and vis versa; therefore, the negative slope (-1.352 μatm yr^{-1}) can be considered as an approximation of the increase trend. In the second around, we applied the LOYO method to the normalized CO_2 by the trend. The residue gives a regression slope of -0.208 μatm yr^{-1} with R^2=0.495 (Supplement Fig. 2b). The process was repeated with data normalized by the sum of previous trends. After three rounds, the slope became negligible (Supplement Fig. 2c). Eventually we obtained a trend of 1.593 μatm yr^{-1}. It is smaller than the trends around 2000 obtained by the iterative regression method since unbalanced sampling makes it impossible for the LOYO method to eliminate overestimate/underestimate by itself.

We applied the LOYO method to the data normalized by the rates in Fig. 1a. A small trend (0.079 μatm yr^{-1}) exists in the biases (Supplement Fig. 3). This trend was added to the rates in Fig. 1a to form the final rates in Table 2 for data normalization. The performance of the three DML models were evaluated by the LOYO method with normalized CO_2. The correlation coefficient R^2 between observations and model predictions is 0.718 for the RF, 0.713 for the GBM, and 0.681 for the FNN; and all three models yielded negligible mean biases (Supplement Fig. 4). In term of training time, the GBM is faster than the RF and the two are much faster than the FNN. A short training time is critical for diagnose analysis and for such a case as rate extraction when many iterations are required for many years. In addition, the RF appeared to be most stable and resistant to overfitting. When the number of data points was much larger than the number of trees, the RF would produce a good result; and when many trees were used, adjusting the number of trees had little effect on the result. The GBM was also resistant to overfitting but less stable than the RF. The FNN was most sensitive to overfitting and took much longer time to train than the RF and GBM. The FNN is also more difficult to configure as the number of hidden layers and neurons, and the number of training iterations could affect the result significantly depending on the number of predictors and data points.

https://doi.org/10.5194/essd-2022-71
Preprint. Discussion started: 11 March 2022


Open Access Earth System Science Data Discussions

We compared the trends of the biases using LOYO with data normalized by the rates in Table 2 and the rate obtained by LOYO above. The results (Fig. 2a) indicate that using a constant rate tends to underestimate CO_2 concentrations in those years that are further apart from the reference year. This would be translated to larger air-sea CO2 fluxes in those years than they would be. The trend became insignificant when the rates in Table 2 were used to normalize CO_2 data (Fig. 2b).

3.2 Flux

Figure 3 shows the annual fluxes of our models and the spatial distribution of the mean fluxes in 1980-2020. The mean fluxes of the biogeochemical models in Global Carbon Budget 2001 (GCB-2021) (Friedlingstein et al., 2021) is also shown in the figure as a reference. The uncertainties of NIES-ML3 (assemble mean of the three models) were calculated by multiplying the mean biases of the three models (Table 2) with the flux change per unit CO_2 change, which is about 0.18 PgC yr^{-1} μatm^{-1} in our study. The flux change with time of NIES-ML3 is parallel to that of GCB-2021. The mean flux of NIES-L3 in 1980-2020 is 1.39 PgC yr^{-1}, which is smaller than the mean flux of GCB_2021 by 0.81 PgC yr^{-1} in the same period. The difference can be attributed to riverine inputs and the sink in coastal areas. The former was estimated to be 0.45±0.18 GtC yr^{-1} by Jacobson et al. (2007) and 0.78±0.41 PgC yr^{-1} by Resplandy et al. (2018). The product of Landschützer et al. (2020) includes CO_2 estimate in the coastal areas. Using their data, we estimated that the costal sink missed by our product is about 0.11 GtC yr^{-1}. By adding this sink and the average riverine input of 0.61 GtC yr^{-1} to the fluxes of NIES-ML3, we estimated that the ocean sink has increase from 1.79±0.47 PgC yr^{-1} in 1980s to 2.58±0.20 PgC yr^{-1} in 2010s with a mean acceleration of 0.027 PgC yr^{-2}.

The spatial distribution patterns of the mean annual flux of NIES-ML3 in 1980-2020 (Fig. 4) agree well with those from GCB-2021 in 2011-2020. In term of flux per unit area, most northern oceans above 30°N appeared to be strong sinks, especially the northern Atlantic. However, strong winter convection and upwelling made the Aleutian Basin a large source. Areas around the tropical zone were mostly strong sources. A large portion of the southern oceans in the 30°S-60°S band absorb atmospheric at the rate of 10 to 20 gC m^{-2} yr^{-1}. Further south, sources and sinks intertwine from region to region. In view of the zonal sum of fluxes, the tropical areas were the net emitter (-0.63 PgC yr^{-1}) with a peak (-0.44 PgC yr^{-1}) at about 4.5°S (Fig. 5). The northern and southern oceans absorbed about 0.93 PgC yr^{-1} and 1.08 PgC yr^{-1} respectively. The North and South temperate zones played as the most important sinks.

3.3 Comparisons

We compared NIES-ML3 with six DML models (Table 3) included GCB-2021. The comparisons are relative, i.e., the fluxes in Fig. 6a-f are not the global sum of the products under comparison but the sum for those grids where both products have data. As each products used different parameters for flux calculation and the choice of different wind products could affect the flux largely (Roobaert et al., 2018), our comparisons focus on the relative changes, not the absolute differences.

https://doi.org/10.5194/essd-2022-71
Preprint. Discussion started: 11 March 2022

The comparison with NIES-NN reals the error potentially existed in products that included a time-dependent linear term in regression or used a constant trend for data normalization. The flux differences are small in 1991-2006, but much larger in early and late years (Fig. 6a). NIES-NN used a constant rate of 1.54 μatm yr^{-1} to normalize data to the reference year set to 2000. Fig. 2a indicate that the differences can be attributed to the underestimates of ocean CO_2. The JMA-MLR product also shows an arch-shaped flux trend (Fig. 6b) as NIES-NN does. Again, the differences are larger in the beginning and ending years than in others. This is expected as the regression method of JMA-MLR includes a linear term of time, which is equivalent to using a constant trend for data normalization.

Instead of using explicit trends to normalize data or including linear term of time in regression, MPI-SOMFFN, CMEMS-FFNN, CSIR-ML6, and OceanSODA-ETHZ used atmospheric CO2 as a predictor so that their regression models could learn the trend implicitly. The day of year is also a predictor of CSIR-ML6. Their comparisons with NIES-ML3 present different patterns (Fig. 6c-f). Except for OceanSODA-ETHZ, the flux differences tend to be smaller in early years and increase with time after 2000. The arch-shaped trend can be detected visually in MPI-SOMFFN, CMEMS-FFNN, and CSIR-ML6 after 1993. The regression models of MPI-SOMFFN, CMEMS-FFNN, and NIES-NN are all FNN. This indicates a FNN can only extract the "correct trend" partially from air CO_2. It is interesting to note that their fluxes around 2000 become close to that of NIES-MLD. The trend of OceanSODA-ETHZ resemble that of NIES-ML3 the most. While OceanSODA-ETHZ and CSIR-ML6 included FNN and GBM (gradient boot machine), the former shows much larger fluxes before 1990. These flux trend patterns could be attributed partly to different clustering and ensemble schemes. JMA-MLR divided the oceans into geographically connected regions; MPI-SOMFFN used a self-organization map to classify data into 16 clusters; CMENS-FFNN is consisted of an ensemble of FNN regressions for randomly selected data in each month, which can be considered as clustering in time; CSIR-ML6 and OceanSODA-ETHZ are consisted of a series of clusters and corresponding regressions of different models.

4. Summary

We have extracted the annual increase rates of ocean CO_2 at decadal scales with three types of machine learning models. The rates appear to track the decadal mean rates of atmospheric CO_2 after 1995. Data scarcity made it difficult to estimate the rates before 1990, but assuming a constant rate proves to be a good approximation as the atmospheric rates show no significant trend. Using the LOYO validation methods with normalized ocean CO_2 data reveals that, in contrast to a constant rate, the time dependent rates significantly reduced the biases of model predictions, especially in the beginning and ending years of the prediction period.

The global annual air-seas fluxes obtained using the reconstructed ocean CO_2 concentrations exhibit a similar long-term trend to that of the mean fluxes of the biogeochemical models of GCB-2021. By adding the sink (0.11 GtC yr^{-1}.) of coastal areas

https://doi.org/10.5194/essd-2022-71
Preprint. Discussion started: 11 March 2022

missed by this study and the riverine input of 0.61 GtC yr^{-1} to the fluxes of this study, we estimated that the ocean sink has increase from 1.79±0.47 PgC yr^{-1} in 1980s to 2.58±0.20 PgC yr^{-1} in 2010s with a mean acceleration of 0.027 PgC yr^{-2}.

The comparisons with six other products included in GCB-2021 indicates that using a constant rate for data normalization or including a linear time-dependent term in regression would overestimate fluxes in the early and late years of the model period, especially when the time spans to a few decades. Embedding implicit rate in regression by using atmospheric CO_2 as a predictor could reduce the bias, but the degree of improvement depends largely on model configuration and data clustering. As our rates can only represent the apparent behaviours of the global oceans at the best and are subjected to uncertainties due to different degrees of data scarcity in each year, further studies from different angles are needed to improve the accuracy of ocean CO_2 flux estimate.

Author contribution

Jiye Zeng: Model experiment design, data processing, and draft layout. Tsunao Matsunaga: Advice on satellite data. Tomoko Shirai: Result checking and advice on carbon budget issues.

Data and Code Availability

The product of reconstructed ocean CO2 fugacity and air-sea fluxes can be accessed at https://db.cger.nies.go.jp/DL/10.17595/20220311.001.html.en under data doi:10.17595/20220311.001 (Zeng, 2022). The supplement material includes the python code for model initialization. As the code was written particularly to work with our data structure, we prefer to provide the complete source upon request so that we can give clear advice case by case.

Acknowledgements

The Surface Ocean CO2 Atlas (SOCAT) is an international effort, endorsed by the International Ocean Carbon Coordination Project (IOCCP), the Surface Ocean Lower Atmosphere Study (SOLAS) and the Integrated Marine Biosphere Research (IMBeR) program, to deliver a uniformly quality-controlled surface ocean CO2 database. The many researchers and funding agencies responsible for the collection of data and quality control are thanked for their contributions to SOCAT.

References

Bakker, D.C.E., Pfeil, B., Landa, C.S., Metzl, N., O'Brien, K.M., Olsen, A., Smith, K., Cosca, C., Harasawa, S., Jones, S.D., Nakaoka, S., Nojiri, Y., Schuster, U., Steinhoff, T., Sweeney, C., Takahashi, T., Tilbrook, B., Wada, C., Wanninkhof, R., Alin, S.R., Balestrini, C.F., Barbero, L., Bates, N.R., Bianchi, A.A., Bonou, F., Boutin, J., Bozec, Y., Burger, E.F., Cai, W.-J., Castle, R.D., Chen, L., Chierici, M., Currie, K., Evans, W., Featherstone, C., Feely, R.A., Fransson, A., Goyet, C.,

https://doi.org/10.5194/essd-2022-71
Preprint. Discussion started: 11 March 2022

Greenwood, N., Gregor, L., Hankin, S., Hardman-Mountford, N.J., Harlay, J., Hauck, J., Hoppema, M., Humphreys, M.P., Hunt, C.W., Huss, B., Ibánhez, J.S.P., Johannessen, T., Keeling, R., Kitidis, V., Körtzinger, A., Kozyr, A., Krasakopoulou, E., Kuwata, A., Landschützer, P., Lauvset, S.K., Lefèvre, N., Lo Monaco, C., Manke, A., Mathis, J.T., Merlivat, L., Millero, F.J., Monteiro, P.M.S., Munro, D.R., Murata, A., Newberger, T., Omar, A.M., Ono, T., Paterson, K., Pearce, D., Pierrot, D., Robbins, L.L., Saito, S., Salisbury, J., Schlitzer, R., Schneider, B., Schweitzer, R., Sieger, R., Skjelvan, I., Sullivan, K.F., Sutherland, S.C., Sutton, A.J., Tadokoro, K., Telszewski, M., Tuma, M., van Heuven, S.M.A.C., Vandemark, D., Ward, B., Watson, A.J., Xu, S.: A multi-decade record of high-quality CO2 data in version 3 of the Surface Ocean CO2 Atlas (SOCAT). Earth Syst. Sci. Data 8, 383–413. https://doi.org/10.5194/essd-8-383-2016, 2016.

Bates, N., Astor, Y., Church, M., Currie, K., Dore, J., Gonaález-Dávila, M., Lorenzoni, L., Muller-Karger, F., Olafsson, J., Santa-Casiano, M., A Time-Series View of Changing Ocean Chemistry Due to Ocean Uptake of Anthropogenic CO2 and Ocean Acidification. oceanog 27, 126–141. https://doi.org/10.5670/oceanog.2014.16, 2014.

Chau, T.T.T., Gehlen, M., Chevallier, F.: A seamless ensemble-based reconstruction of surface ocean pCO2 and air–sea CO2 fluxes over the global coastal and open oceans. Biogeochemistry: Air - Sea Exchange. https://doi.org/10.5194/bg-2021-207, 2021.

Conway, T.J., Tans, P.P., Waterman, L.S., Thoning, K.W., Kitzis, D.R., Masarie, K.A., Zhang, N., Evidence for interannual variability of the carbon cycle from the National Oceanic and Atmospheric Administration/Climate Monitoring and Diagnostics Laboratory Global Air Sampling Network. J. Geophys. Res. 99, 22831. https://doi.org/10.1029/94JD01951, 1994.

Denvil-Sommer, A., Gehlen, M., Vrac, M., Mejia, C.: LSCE-FFNN-v1: a two-step neural network model for the reconstruction of surface ocean CO2 over the global ocean. Geosci. Model Dev. 12, 2091–2105. https://doi.org/10.5194/gmd-12-2091-2019, 2019.

Dlugokencky, E.J., Thoning, K.W., Lang P.M., and Tans , P.P.: NOAA Greenhouse Gas Reference from Atmospheric Carbon Dioxide Dry Air Mole Fractions from the NOAA ESRL Carbon Cycle Cooperative Global Air Sampling Network, 2019.

Fay, A.R., McKinley, G.A., Global trends in surface ocean pCO2 from in situ data: GLOBAL TRENDS IN SURFACE OCEAN pCO2. Global Biogeochem. Cycles 27, 541–557. https://doi.org/10.1002/gbc.20051, 2013.

Friedlingstein, P., O'Sullivan, M., Jones, M.W., Andrew, R.M., Hauck, J., Olsen, A., Peters, G.P., Peters, W., Pongratz, J., Sitch, S., Le Quéré, C., Canadell, J.G., Ciais, P., Jackson, R.B., Alin, S., Aragão, L.E.O.C., Arneth, A., Arora, V., Bates, N.R., Becker, M., Benoit-Cattin, A., Bittig, H.C., Bopp, L., Bultan, S., Chandra, N., Chevallier, F., Chini, L.P., Evans, W., Florentie, L., Forster, P.M., Gasser, T., Gehlen, M., Gilfillan, D., Gkritzalis, T., Gregor, L., Gruber, N., Harris, I., Hartung, K., Haverd, V., Houghton, R.A., Ilyina, T., Jain, A.K., Joetzjer, E., Kadono, K., Kato, E., Kitidis, V., Korsbakken, J.I., Gloege, L., McKinley, G.A., Landschützer, P., Fay, A.R., Frölicher, T.L., Fyfe, J.C., Ilyina, T., Jones, S., Lovenduski, N.S., Rodgers, K.B., Schlunegger, S., Takano, Y., Quantifying Errors in Observationally Based Estimates of Ocean Carbon Sink Variability. Global Biogeochem Cycles 35. https://doi.org/10.1029/2020GB006788, 2021.

Gloege, L., McKinley, G.A., Landschützer, P., Fay, A.R., Frölicher, T.L., Fyfe, J.C., Ilyina, T., Jones, S., Lovenduski, N.S., Rodgers, K.B., Schlunegger, S., Takano, Y., Quantifying Errors in Observationally Based Estimates of Ocean Carbon Sink Variability. Global Biogeochem Cycles 35. https://doi.org/10.1029/2020GB006788, 2021.

Gregor, L., Lebehot, A.D., Kok, S., Scheel Monteiro, P.M., A comparative assessment of the uncertainties of global surface ocean CO2 estimates using a machine-learning ensemble (CSIR-ML6 version 2019a) – have we hit the wall? Geosci. Model Dev. 12, 5113–5136. https://doi.org/10.5194/gmd-12-5113-2019, 2019.

https://doi.org/10.5194/essd-2022-71
Preprint. Discussion started: 11 March 2022

Gregor, L., Gruber, N.: OceanSODA-ETHZ: a global gridded data set of the surface ocean carbonate system for seasonal to decadal studies of ocean acidification. Earth Syst. Sci. Data 13, 777–808. https://doi.org/10.5194/essd-13-777-2021, 2021.

Hu, C., Lee, Z., Franz, B.: Chlorophyll-a algorithms for oligotrophic oceans: A novel approach based on three-band reflectance difference: A NOVEL OCEAN CHLOROPHYLL a ALGORITHM. J. Geophys. Res. 117. https://doi.org/10.1029/2011JC007395, 2012.

Iida, Y., Kojima, A., Takatani, Y., Nakano, T., Sugimoto, H., Midorikawa, T., Ishii, M.: Trends in pCO2 and sea–air CO2 flux over the global open oceans for the last two decades. J Oceanogr 71, 637–661. https://doi.org/10.1007/s10872-015-0306-4, 2015.

Iida, Y., Takatani, Y., Kojima, A., Ishii, M., Global trends of ocean CO2 sink and ocean acidification: an observation-based reconstruction of surface ocean inorganic carbon variables. J Oceanogr 77, 323–358. https://doi.org/10.1007/s10872-020-00571-5, 2021.

Ishii, M., Shouji, A., Sugimoto, S., Matsumoto, T. Objective analyses of sea-surface temperature and marine meteorological variables for the 20th century using ICOADS and the Kobe Collection. Int. J. Climatol. 25, 865–879. https://doi.org/10.1002/joc.1169, 2005.

Ishwaran, H.: The effect of splitting on random forests. Mach Learn 99, 75–118. https://doi.org/10.1007/s10994-014-5451-2, 2015.

Jacobson, A.R., Mikaloff Fletcher, S.E., Gruber, N., Sarmiento, J.L., Gloor, M., A joint atmosphere-ocean inversion for surface fluxes of carbon dioxide: 1. Methods and global-scale fluxes: JOINT INVERSION-METHODS AND GLOBAL FLUXES. Global Biogeochem. Cycles 21. https://doi.org/10.1029/2005GB002556, 2007.

Jones, S.D., Le Quéré, C., Rödenbeck, C., Manning, A.C., Olsen, A., A statistical gap-filling method to interpolate global monthly surface ocean carbon dioxide data: STATISTICAL INTERPOLATION OF OCEAN CO2. J. Adv. Model. Earth Syst. 7, 1554–1575. https://doi.org/10.1002/2014MS000416, 2015.

Ke, G., Meng, Q., Finley, T., Wang, T., Chen, W., Ma, W., Ye, Q., Liu, T.-Y., LightGBM: A Highly Efficient Gradient Boosting Decision Tree 9. Advances in Neural Information Processing Systems, 30, 3146–3154. 2017.

Khatiwala, S., Tanhua, T., Mikaloff Fletcher, S., Gerber, M., Doney, S.C., Graven, H.D., Gruber, N., McKinley, G.A., Murata, A., Ríos, A.F., Sabine, C.L.: Global ocean storage of anthropogenic carbon. Biogeosciences 10, 2169–2191. https://doi.org/10.5194/bg-10-2169-2013, 2013.

Landschützer, P., Gruber, N., Bakker, D.C.E., Schuster, U., Nakaoka, S., Payne, M.R., Sasse, T.P., Zeng, J., A neural network-based estimate of the seasonal to inter-annual variability of the Atlantic Ocean carbon sink. Biogeosciences 10, 7793–7815. https://doi.org/10.5194/bg-10-7793-2013, 2013.

Landschützer, P., Gruber, N., Bakker, D.C.E.: Decadal variations and trends of the global ocean carbon sink: DECADAL AIR-SEA CO2 FLUX VARIABILITY. Global Biogeochem. Cycles 30, 1396–1417. https://doi.org/10.1002/2015GB005359, 2016.

Landschützer, P., Lefèvre, N., Lenton, A., Lienert, S., Liu, Z., Lombardozzi, D., Marland, G., Metzl, N., Munro, D.R., Nabel, J.E.M.S., Nakaoka, S.-I., Niwa, Y., O'Brien, K., Ono, T., Palmer, P.I., Pierrot, D., Poulter, B., Resplandy, L., Robertson, E., Rödenbeck, C., Schwinger, J., Séférian, R., Skjelvan, I., Smith, A.J.P., Sutton, A.J., Tanhua, T., Tans, P.P., Tian, H., Tilbrook, B., van der Werf, G., Vuichard, N., Walker, A.P., Wanninkhof, R., Watson, A.J., Willis, D., Wiltshire, A.J., Yuan, W., Yue, X., Zaehle, S.: Global Carbon Budget 2020. Earth Syst. Sci. Data 12, 3269–3340.

https://doi.org/10.5194/essd-12-3269-2020, 2020.

Laruelle, G.G., Landschützer, P., Gruber, N., Tison, J.-L., Delille, B., Regnier, P., Global high-resolution monthly pCO2 climatology for the coastal ocean derived from neural network interpolation. Biogeosciences 14, 4545–4561. https://doi.org/10.5194/bg-14-4545-2017, 2017.

McKinley, G.A., Fay, A.R., Takahashi, T., Metzl, N., Convergence of atmospheric and North Atlantic carbon dioxide trends on multidecadal timescales. Nature Geosci 4, 606–610. https://doi.org/10.1038/ngeo1193, 2011.

McKinley, G.A., Pilcher, D.J., Fay, A.R., Lindsay, K., Long, M.C., Lovenduski, N.S.: Timescales for detection of trends in the ocean carbon sink. Nature 530, 469–472. https://doi.org/10.1038/nature16958, 2016.
(Our findings suggest that, owing to large internal climate variability, it is unlikely that changes in the rate of anthropogenic carbon uptake can be directly observed in most oceanic regions at present, but that this may become possible between 2020 and 2050 in some regions)

Nakaoka, S., Telszewski, M., Nojiri, Y., Yasunaka, S., Miyazaki, C., Mukai, H., Usui, N., Estimating temporal and spatial variation of ocean surface pCO2 in the North Pacific using a self-organizing map neural network technique. Biogeosciences 10, 6093–6106. https://doi.org/10.5194/bg-10-6093-2013, 2013.

Natekin, A. and Knoll, A.: Gradient boosting machines, a tutorial. Front. Neurorobot. 7. https://doi.org/10.3389/fnbot.2013.00021, 2013.

Pfeil, B., Olsen, A., Bakker, D.C.E., Hankin, S., Koyuk, H., Kozyr, A., Malczyk, J., Manke, A., Metzl, N., Sabine, C.L., Akl, J., Alin, S.R., Bates, N., Bellerby, R.G.J., Borges, A., Boutin, J., Brown, P.J., Cai, W.-J., Chavez, F.P., Chen, A., Cosca, C., Fassbender, A.J., Feely, R.A., González-Dávila, M., Goyet, C., Hales, B., Hardman-Mountford, N., Heinze, C., Hood, M., Hoppema, M., Hunt, C.W., Hydes, D., Ishii, M., Johannessen, T., Jones, S.D., Key, R.M., Körtzinger, A., Landschützer, P., Lauvset, S.K., Lefèvre, N., Lenton, A., Lourantou, A., Merlivat, L., Midorikawa, T., Mintrop, L., Miyazaki, C., Murata, A., Nakadate, A., Nakano, Y., Nakaoka, S., Nojiri, Y., Omar, A.M., Padin, X.A., Park, G.-H., Paterson, K., Perez, F.F., Pierrot, D., Poisson, A., Ríos, A.F., Santana-Casiano, J.M., Salisbury, J., Sarma, V.V.S.S., Schlitzer, R., Schneider, B., Schuster, U., Sieger, R., Skjelvan, I., Steinhoff, T., Suzuki, T., Takahashi, T., Tedesco, K., Telszewski, M., Thomas, H., Tilbrook, B., Tjiputra, J., Vandemark, D., Veness, T., Wanninkhof, R., Watson, A.J., Weiss, R., Wong, C.S., Yoshikawa-Inoue, H., A uniform, quality controlled Surface Ocean CO2 Atlas (SOCAT). Earth Syst. Sci. Data 5, 125–143. https://doi.org/10.5194/essd-5-125-2013, 2013.

Resplandy, L., Keeling, R.F., Rödenbeck, C., Stephens, B.B., Khatiwala, S., Rodgers, K.B., Long, M.C., Bopp, L., Tans, P.P., Revision of global carbon fluxes based on a reassessment of oceanic and riverine carbon transport. Nature Geosci 11, 504–509. https://doi.org/10.1038/s41561-018-0151-3, 2018.

Roobaert, A., Laruelle, G.G., Landschützer, P., Regnier, P., Uncertainty in the global oceanic CO2 uptake induced by wind forcing: quantification and spatial analysis. Biogeosciences 15, 1701–1720. https://doi.org/10.5194/bg-15-1701-2018, 2018.

Sabine, C.L.: The Oceanic Sink for Anthropogenic CO2. Science 305, 367–371. https://doi.org/10.1126/science.1097403, 2004.

Sabine, C.L., Hankin, S., Koyuk, H., Bakker, D.C.E., Pfeil, B., Olsen, A., Metzl, N., Kozyr, A., Fassbender, A., Manke, A., Malczyk, J., Akl, J., Alin, S.R., Bellerby, R.G.J., Borges, A., Boutin, J., Brown, P.J., Cai, W.-J., Chavez, F.P., Chen, A., Cosca, C., Feely, R.A., González-Dávila, M., Goyet, C., Hardman-Mountford, N., Heinze, C., Hoppema, M., Hunt, C.W., Hydes, D., Ishii, M., Johannessen, T., Key, R.M., Körtzinger, A., Landschützer, P., Lauvset, S.K., Lefèvre, N., Lenton, A., Lourantou, A., Merlivat, L., Midorikawa, T., Mintrop, L., Miyazaki, C., Murata, A., Nakadate, A., Nakano, Y., Nakaoka, S., Nojiri, Y., Omar, A.M., Padin, X.A., Park, G.-H., Paterson, K., Perez, F.F., Pierrot, D., Poisson, A., Ríos, A.F., Salisbury, J.,

https://doi.org/10.5194/essd-2022-71
Preprint. Discussion started: 11 March 2022

Santana-Casiano, J.M., Sarma, V.V.S.S., Schlitzer, R., Schneider, B., Schuster, U., Sieger, R., Skjelvan, I., Steinhoff, T., Suzuki, T., Takahashi, T., Tedesco, K., Telszewski, M., Thomas, H., Tilbrook, B., Vandemark, D., Veness, T., Watson, A.J., Weiss, R., Wong, C.S., Yoshikawa-Inoue, H.: Surface Ocean CO2 Atlas (SOCAT) gridded data products. Earth Syst. Sci. Data 5, 145–153. https://doi.org/10.5194/essd-5-145-2013, 2013.

Sasse, T.P., McNeil, B.I., Abramowitz, G., A new constraint on global air-sea CO2 fluxes using bottle carbon data: DATA-BASED CONTEMPORARY CO2 UPTAKE. Geophys. Res. Lett. 40, 1594–1599. https://doi.org/10.1002/grl.50342, 2013.

Sasse, T.P., McNeil, B.I., Abramowitz, G., A novel method for diagnosing seasonal to inter-annual surface ocean carbon dynamics from bottle data using neural networks (preprint). Biogeochemistry: Open Ocean. https://doi.org/10.5194/bgd-9-15329-2012, 2012.

Sasse, T.P., McNeil, B.I., Abramowitz, G., A new constraint on global air-sea CO2 fluxes using bottle carbon data: DATA-BASED CONTEMPORARY CO2 UPTAKE. Geophys. Res. Lett. 40, 1594–1599. https://doi.org/10.1002/grl.50342, 2013.

Sutton, A.J., Feely, R.A., Maenner-Jones, S., Musielwicz, S., Osborne, J., Dietrich, C., Monacci, N., Cross, J., Bott, R., Kozyr, A., Andersson, A.J., Bates, N.R., Cai, W.-J., Cronin, M.F., De Carlo, E.H., Hales, B., Howden, S.D., Lee, C.M., Manzello, D.P., McPhaden, M.J., Meléndez, M., Mickett, J.B., Newton, J.A., Noakes, S.E., Noh, J.H., Olafsdottir, S.R., Salisbury, J.E., Send, U., Trull, T.W., Vandemark, D.C., Weller, R.A., Autonomous seawater pCO2 and pH time series from 40 surface buoys and the emergence of anthropogenic trends. Earth Syst. Sci. Data 11, 421–439. https://doi.org/10.5194/essd-11-421-2019, 2019.

Svozil, D., Kvasnicka, V., Pospichal, J., Introduction to multi-layer feed-forward neural networks. Chemometrics and Intelligent Laboratory Systems 39, 43–62. https://doi.org/10.1016/S0169-7439(97)00061-0, 1997.

Takahashi, T., Sutherland, S.C., Wanninkhof, R., Sweeney, C., Feely, R.A., Chipman, D.W., Hales, B., Friederich, G., Chavez, F., Sabine, C., Watson, A., Bakker, D.C.E., Schuster, U., Metzl, N., Yoshikawa-Inoue, H., Ishii, M., Midorikawa, T., Nojiri, Y., Körtzinger, A., Steinhoff, T., Hoppema, M., Olafsson, J., Arnarson, T.S., Tilbrook, B., Johannessen, T., Olsen, A., Bellerby, R., Wong, C.S., Delille, B., Bates, N.R., de Baar, H.J.W., Climatological mean and decadal change in surface ocean pCO2, and net sea–air CO2 flux over the global oceans. Deep Sea Research Part II: Topical Studies in Oceanography 56, 554–577. https://doi.org/10.1016/j.dsr2.2008.12.009, 2009.

Wanninkhof, R., Relationship between wind speed and gas exchange over the ocean revisited: Gas exchange and wind speed over the ocean. Limnol. Oceanogr. Methods 12, 351–362. https://doi.org/10.4319/lom.2014.12.351, 2014.

Watson, A.J., Schuster, U., Shutler, J.D., Holding, T., Ashton, I.G.C., Landschützer, P., Woolf, D.K., Goddijn-Murphy, L., Revised estimates of ocean-atmosphere CO2 flux are consistent with ocean carbon inventory. Nat Commun 11, 4422. https://doi.org/10.1038/s41467-020-18203-3, 2020.

Weiss, R.F., Carbon dioxide in water and seawater: the solubility of a non-ideal gas. Marine Chemistry 2, 203–215. https://doi.org/10.1016/0304-4203(74)90015-2, 1974.

Wright, M.N., Ziegler, A., ranger: A Fast Implementation of Random Forests for High Dimensional Data in C++ and R. J. Stat. Soft. 77. https://doi.org/10.18637/jss.v077.i01, 2017.

Zeng, J., Nojiri, Y., Landschützer, P., Telszewski, M., Nakaoka, S.: A Global Surface Ocean fCO2 Climatology Based on a Feed-Forward Neural Network. Journal of Atmospheric and Oceanic Technology 31, 1838–1849. https://doi.org/10.1175/JTECH-D-13-00137.1, 2014.

Zeng, J., Matsunaga, T., Saigusa, N., Shirai, T., Nakaoka, S., Tan, Z.-H.: Technical note: Evaluation of three machine learning models for surface ocean CO2 mapping. Ocean Sci. 13, 303–313. https://doi.org/10.5194/os-13-303-2017, 2017.

https://doi.org/10.5194/essd-2022-71
Preprint. Discussion started: 11 March 2022

480 Zeng, J., Matsunaga, T., Tan, Z.-H., Saigusa, N., Shirai, T., Tang, Y., Peng, S., Fukuda, Y.: Global terrestrial carbon fluxes of 1999–2019 estimated by upscaling eddy covariance data with a random forest. Sci Data 7, 313. https://doi.org/10.1038/s41597-020-00653-5, 2020.

Zeng, J.: NIES-ML3 ensemble product of surface ocean CO2 concentrations and air-sea CO2 fluxes reconstructed by using
485 three machine learning models with new CO2 trends. https://db.cger.nies.go.jp/DL/10.17595/20220311.001.html.en, 2022

Zweng, M. M, Reagan, J. R., Seidov, D., Boyer, T. P., Locarnini, R. A., Garcia, H. E., Mishonov, A. V., Baranova, O. K., Paver, C. R., Weathers, K. W., Smolyar, I.: World Ocean Atlas 2018, Volume 2: Salinity. A. Mishonov, technical editor, NOAA Atlas NESDIS 82, 50pp, 2019

490

https://doi.org/10.5194/essd-2022-71
Preprint. Discussion started: 11 March 2022

Open Access Earth System Science Data Discussions

Table 1. Data sources. CO2W: ocean CO_2 fugacity. pCO2A: mole fraction ratio of atmospheric CO_2. CHL: chlorophyll-a concentration; SST: sea surface temperature. SSS: sea surface salinity. MLD: mix layer depth. WIND: wind speed. Ps: surface pressure.

Variable	Units	*Resolutions*	Source URL	DOI or Version	Reference
CO2W	μatm	Monthly, 1×1 degree.	https://www.socat.info/	Version-2021	Sabine et al., 2013; Pfeil et al., 2013; Bakker et al., 2016.
pCO2A	ppm	Monthly, 0.05 sine latitude.	https://www.esrl.noaa.gov/gmd/ccgg/mbl/		Conway et al., 1994 and Dlugokencky et al., 2019
CHL	mg m^{-3}	Monthly climatology, 0.083x0.083 degree.	https://oceancolor.gsfc.nasa.gov/cgi/l3	10.5067/AQUA/MODIS/L3M/CHL/2018	Hu et al., 2012.
SST	°C	Monthly, 1×1 degree.	https://psl.noaa.gov/data/gridded/data.cobe.html http://ds.data.jma.go.jp/tcc/tcc/library/MRCS_SV12/explanation/cobe_sst_e.htm		Ishii et al., 2005.
SSS	g g^{-3}	Monthly climatology, 1×1 degree.	https://www.nodc.noaa.gov/OC5/woa18/woa18data.html		Zweng et a., 2019
MLD	m	Monthly climatology, 1×1 degree.	https://www.nodc.noaa.gov/OC5/woa18/woa18data.html		
WIND	m s^{-1}	Monthly, 0.25×0.25 degree.	https://cds.climate.copernicus.eu/cdsapp#!/dataset/reanalysis-era5-single-levels-monthly-means?tab=form	10.24381/CDS.F17050D7	
Ps	m s^{-1}	Monthly, 0.25×0.25 degree.	Same as WIND	Same as WIND	

495

https://doi.org/10.5194/essd-2022-71
Preprint. Discussion started: 11 March 2022

Open Access Earth System Science Data Discussions

Table 2. Annual rates and LOYO validation results. Rate: rates used for data normalization and CO_2 reconstruction. Bias: prediction minus observation. STD: standard deviation of the biases. R^2: correlation coefficient between prediction and observation. ND: number of data points.

Year	Rate	RF			GBM			FNN			ND
	(μatm yr^{-1})	Bias (μatm)	STD (μatm)	R^2	Bias (μatm)	STD (μatm)	R^2	Bias (μatm)	STD (μatm)	R^2	
1980	1.538	-3.459	11.397	0.895	-3.087	12.092	0.885	-5.776	13.386	0.843	339
1981	1.538	1.344	11.708	0.879	1.425	12.615	0.860	0.328	11.963	0.875	610
1982	1.538	1.998	15.532	0.551	2.268	16.528	0.491	3.789	18.017	0.380	441
1983	1.538	-2.270	16.289	0.573	-2.158	16.049	0.586	-2.601	19.640	0.381	273
1984	1.538	0.650	18.233	0.629	0.108	18.117	0.634	-1.274	19.106	0.592	504
1985	1.538	3.560	15.113	0.586	3.672	15.846	0.545	2.801	14.897	0.605	708
1986	1.538	1.586	16.624	0.703	2.406	17.779	0.657	1.408	14.836	0.763	897
1987	1.538	1.824	15.941	0.504	1.019	16.138	0.496	0.815	17.260	0.425	1587
1988	1.538	-4.016	13.229	0.823	-3.035	13.772	0.816	-4.924	14.930	0.771	1010
1989	1.538	-3.950	27.739	0.538	-2.384	29.272	0.492	-6.740	31.099	0.404	1117
1990	1.538	-3.613	12.049	0.837	-3.602	12.243	0.832	-3.557	12.343	0.830	889
1991	1.553	0.490	12.588	0.811	0.365	13.004	0.799	-0.625	13.885	0.770	2011
1992	1.539	3.834	15.136	0.620	3.623	15.951	0.583	3.498	17.087	0.526	2521
1993	1.576	1.145	15.751	0.737	1.035	16.128	0.725	1.761	16.953	0.694	3398
1994	1.605	-3.205	20.712	0.731	-2.384	21.430	0.715	-4.036	22.130	0.690	3981
1995	1.577	-1.780	19.298	0.652	-1.800	19.243	0.654	-0.480	19.812	0.636	6157
1996	1.599	-1.459	20.418	0.729	-1.011	20.605	0.725	-2.446	21.740	0.691	6091
1997	1.613	2.503	22.817	0.734	2.733	23.337	0.721	2.707	24.357	0.697	4335
1998	1.698	1.683	21.860	0.556	1.976	22.959	0.510	2.907	23.859	0.467	5860
1999	1.749	-2.124	21.757	0.693	-1.425	22.678	0.669	-3.816	23.640	0.632	4081
2000	1.794	-3.090	26.342	0.599	-2.533	27.194	0.575	-1.595	27.883	0.556	4656
2001	1.804	-4.300	23.231	0.705	-3.778	22.703	0.720	-4.469	24.230	0.679	4855
2002	1.808	0.600	18.504	0.674	0.540	18.315	0.680	0.407	19.884	0.623	6760
2003	1.813	-0.481	18.796	0.660	-0.688	19.522	0.633	-2.296	20.726	0.582	7001
2004	1.822	0.481	16.927	0.746	0.664	17.338	0.733	1.103	18.128	0.707	8077
2005	1.848	-1.180	16.819	0.760	-1.077	17.015	0.755	0.156	18.415	0.714	9575
2006	1.861	0.478	18.753	0.765	0.547	18.767	0.765	0.873	20.518	0.718	12192
2007	1.861	-0.132	20.361	0.688	-0.472	20.152	0.695	-0.302	22.100	0.633	12326
2008	1.905	0.308	20.295	0.741	0.473	20.552	0.734	0.220	21.776	0.701	11524
2009	1.930	2.498	20.484	0.691	2.093	20.557	0.690	3.551	22.125	0.635	11571
2010	1.942	0.717	18.485	0.720	0.539	18.761	0.712	0.449	19.973	0.674	12822
2011	2.022	1.477	22.692	0.681	1.642	22.803	0.677	3.442	23.392	0.655	13353
2012	2.082	-0.502	22.875	0.682	-0.726	22.952	0.680	-0.675	23.389	0.667	13393
2013	2.159	-0.697	21.486	0.695	-0.725	22.075	0.678	-0.238	22.101	0.678	11366
2014	2.283	3.069	23.902	0.682	2.469	23.288	0.700	2.539	25.135	0.651	13445
2015	2.357	-1.954	22.905	0.708	-2.217	23.017	0.705	-2.025	24.323	0.671	13153
2016	2.395	-0.634	17.929	0.773	-0.647	18.117	0.768	0.185	18.945	0.747	14915
2017	2.420	0.163	19.695	0.769	0.005	19.700	0.769	1.794	21.663	0.719	14693
2018	2.422	0.634	20.126	0.704	0.373	20.387	0.697	0.430	22.574	0.628	12098
2019	2.455	-1.513	20.551	0.727	-1.628	20.265	0.734	-2.131	22.488	0.672	11416
2020	2.431	-0.354	22.937	0.719	-0.056	22.848	0.721	-0.560	24.389	0.682	7433

500

https://doi.org/10.5194/essd-2022-71
Preprint. Discussion started: 11 March 2022

Open Access Earth System Science Data Discussions

Table 3. Datasets for comparison. Machine learning models include random forest (RF), gradient boost machine (GBM), feedforward neural network (FNN), Support vector machine for regression (SVR) and multiple linear regression (MLR). Predictors include atmospheric CO_2 (COA), ocean CO_2 climatology (CO2C), sea surface temperature (SST), sea surface temperature anomaly (dSST), sea surface salinity (SSS), sea surface height (SSH), chlorophyll-a (CHL), chlorophyll-a anomaly (dCHL), mixed layer depth (MLD), wind speed (WIND), time (TIME), latitude (LAT), and latitude (LON).

Dataset	Period	Reference	Regression	Trend	Clustering	Predictors
NIES-ML3	1980-2020	This study	RL, GBM, and FNN.	Year dependent rates	1 global cluster. CO2 normalized to 2000 using variable annual rates	SST, dSST, SSS, CHL, MLD, LAT, LON.
NIES-NN	1980-2020	Zeng et al. (2014). (doi:10.17595/20210806.001)	FNN	A linear trend	1 global cluster. CO2 normalized to 2000 using rate of 1.54 μatm yr-1.	SST, SSS, CHL, MLD, dSST.
JMA-MLR	1990-2020	Iida et al. (2021) https://www.data.jma.go.jp/gmd/kaiyou/english/co2_flux/co2_flux_data_en.html	MLR	Cluster dependent linear trends	Manually defined clusters by regions.	SST, SSS, SSH, CHL, MLD, TIME.
MPI-SOMFFN	1982-2019	Landschützer et al. (2016). (https://www.ncei.noaa.gov/data/oceans/ncei/ocads/data/0160558/MPI_SOM-FFN_v2021/)	FNN	Implicit rates learned from air CO2	16 clusters by self-organization map.	SST, SSS, MLD, CHL, CO2A.
CMEMS-FFNN	1985-2019	Chau et al. (2021). (https://resources.marine.copernicus.eu/?option=com_csw&view=details&product_id=MULTIOBS_GLO_BIO_CARBON_SURFACE_REP_015_008)	FNN	Implicit rates learned from air CO2	Clustering by month with a window size of three months.	SST, SSS, SSH, MLD, CHL, CO2A, CO2C, LAT, LON.
CSIR-ML6	1982-2016	Gregor et al. (2019) (https://www.ncei.noaa.gov/access/metadata/landing-page/bin/iso?id=gov.noaa.nodc:0206205)	GBM, FNN, SVR, and RF	Implicit rates learned from air CO2 and time	Repetition of K-mean clustering and CO2 biomes clustering	SST, dSST, SSS, MLD, CHL, dCHL, WIND, CO2A, TIME.
OceanSODA-ETHZ	1982-2020	Gregor and Gruber (2021). (https://doi.org/10.25921/m5wx-ja34)	GBM and FNN	Implicit rates learned from air CO2	Repetition of K-mean clustering.	SST, SSS, CHL, MLD, WIND, CO2A.

https://doi.org/10.5194/essd-2022-71
Preprint. Discussion started: 11 March 2022

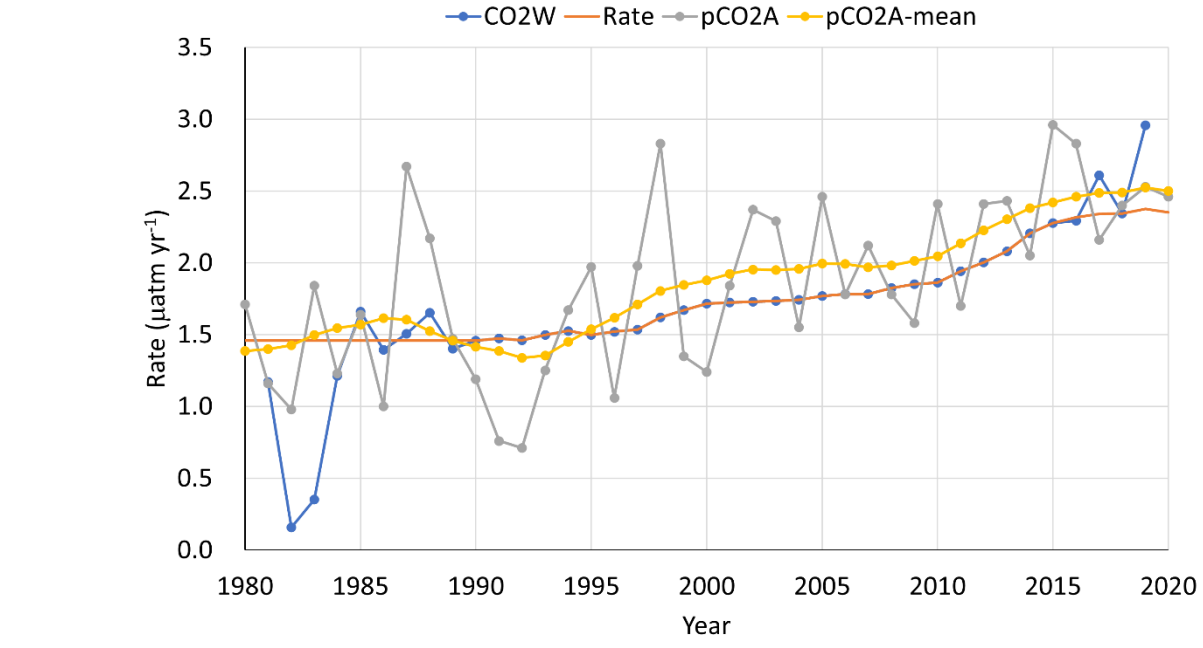

(a)

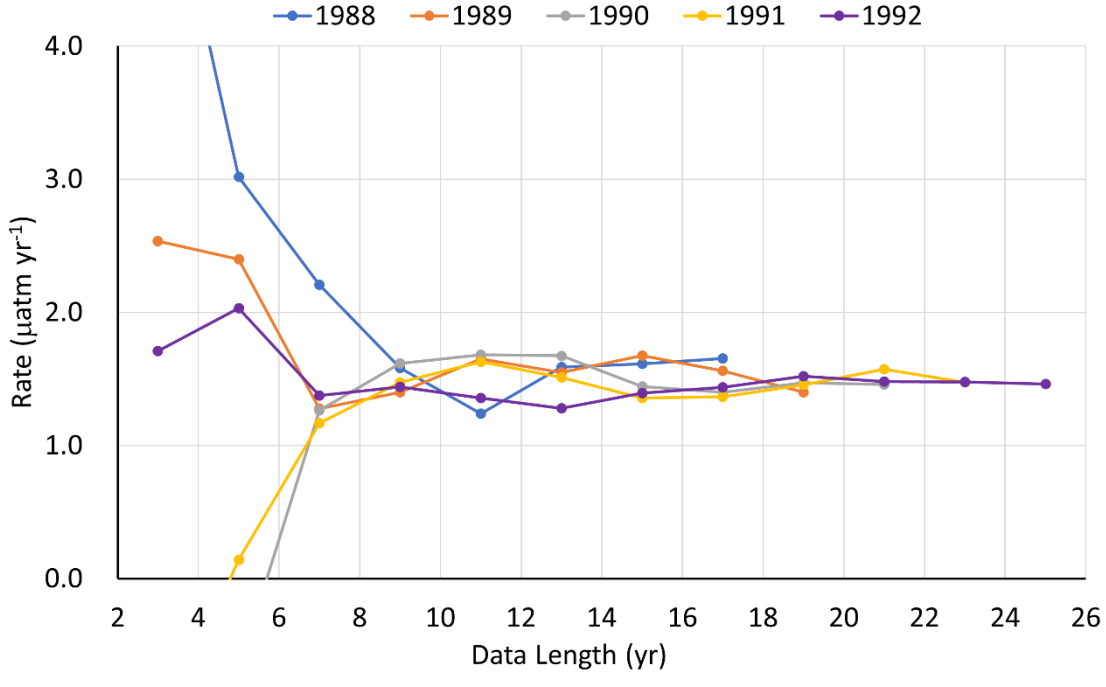

(b)

https://doi.org/10.5194/essd-2022-71
Preprint. Discussion started: 11 March 2022

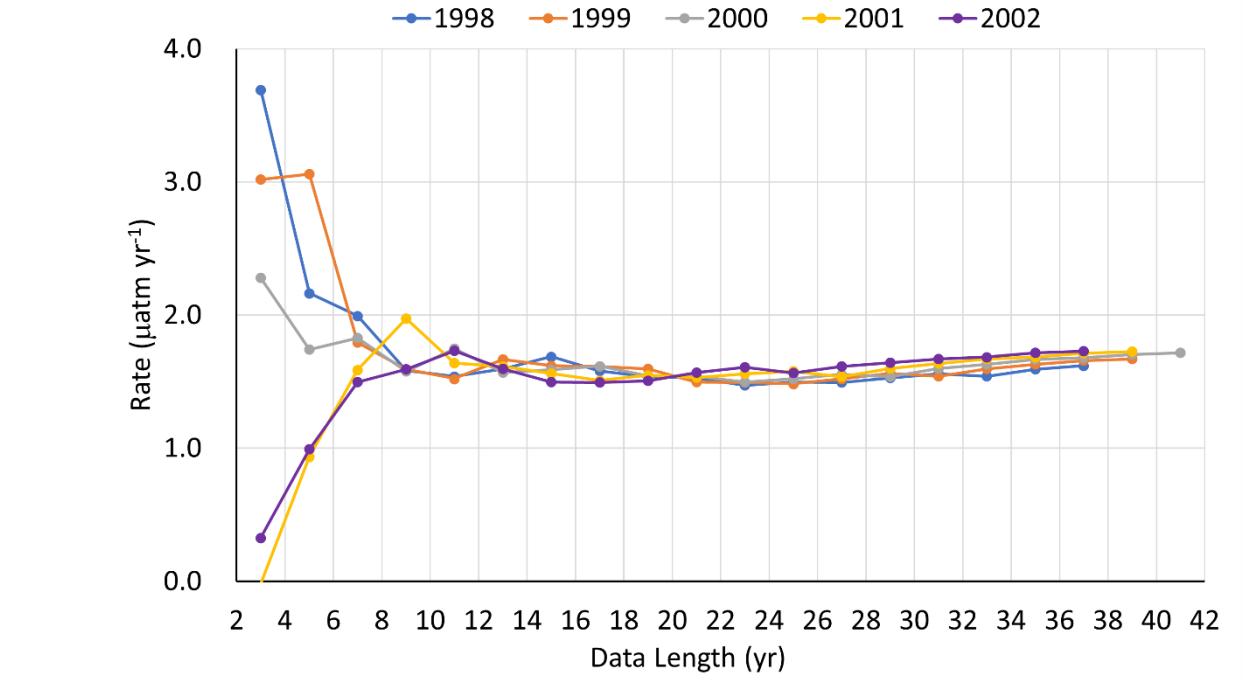

(c)

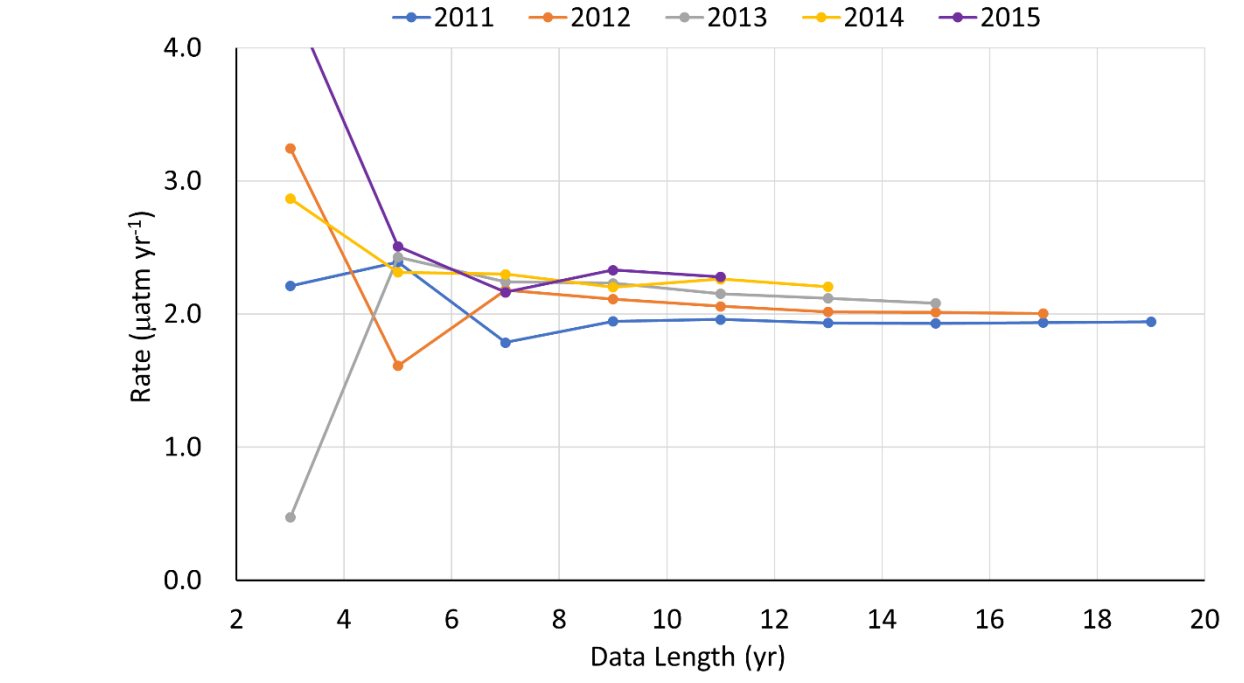

(d)

https://doi.org/10.5194/essd-2022-71
Preprint. Discussion started: 11 March 2022

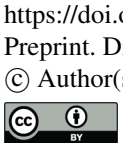

Open Access Earth System Science Data Discussions

515 **Figure 1: Annual increase rate of CO_2. (a): the annual increate rate (blue) for a target year was estimated by using the iteration method with the longest data length around the year; the rates used for normalization (orange) are the same as those in blue except for the period when data are insufficient; the annual increase rates of atmospheric CO_2 (grey) and decadal means (yellow) are presented as references. (b)-(c) demonstrates the variations of the rates with data length and the difficulty of choosing the optimal length.**

520

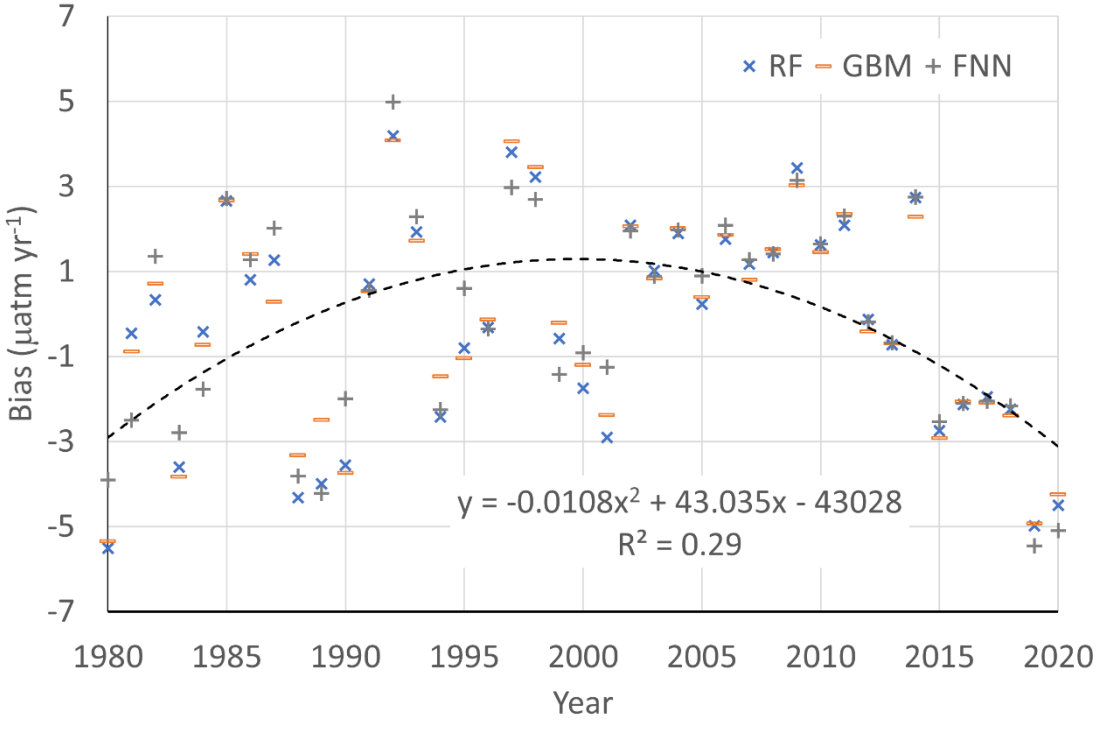

(a)

https://doi.org/10.5194/essd-2022-71
Preprint. Discussion started: 11 March 2022

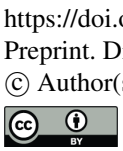

Open Access Earth System Science Data Discussions

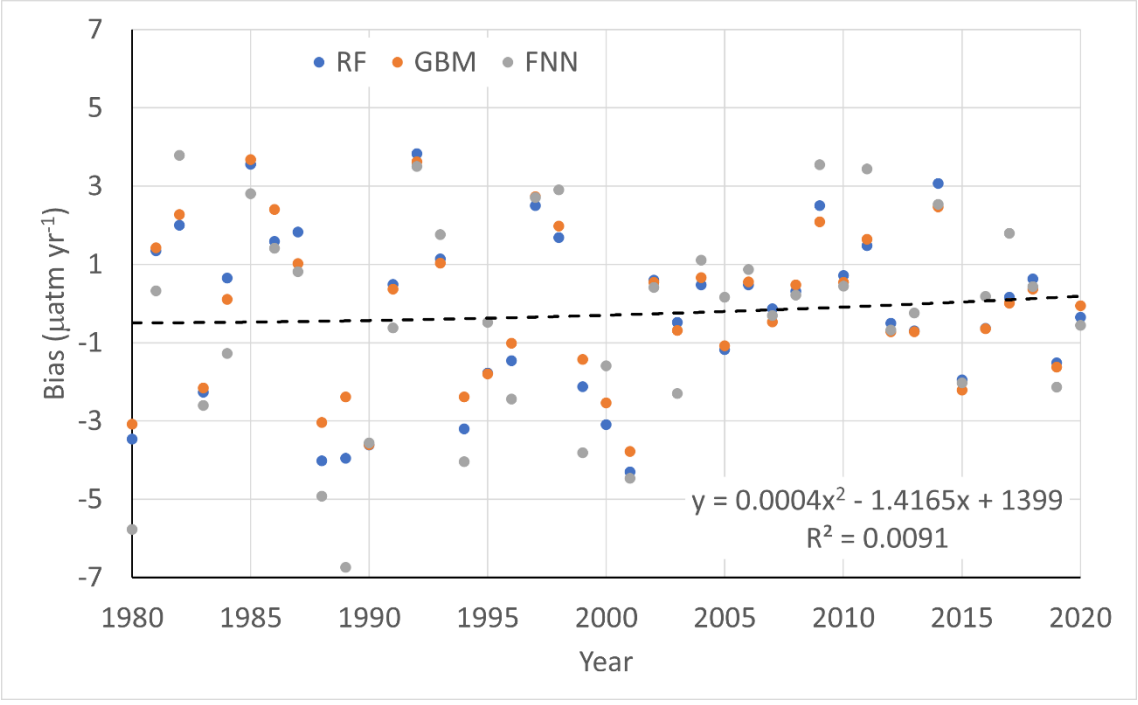

(b)

Figure 2: Trend of LOYO biases: (a) results of applying LOYO to data normalized with a constant rate of 1.593 µatm yr^{-1}. (b) results of applying LOYO to data normalized with the rates in Table 2.

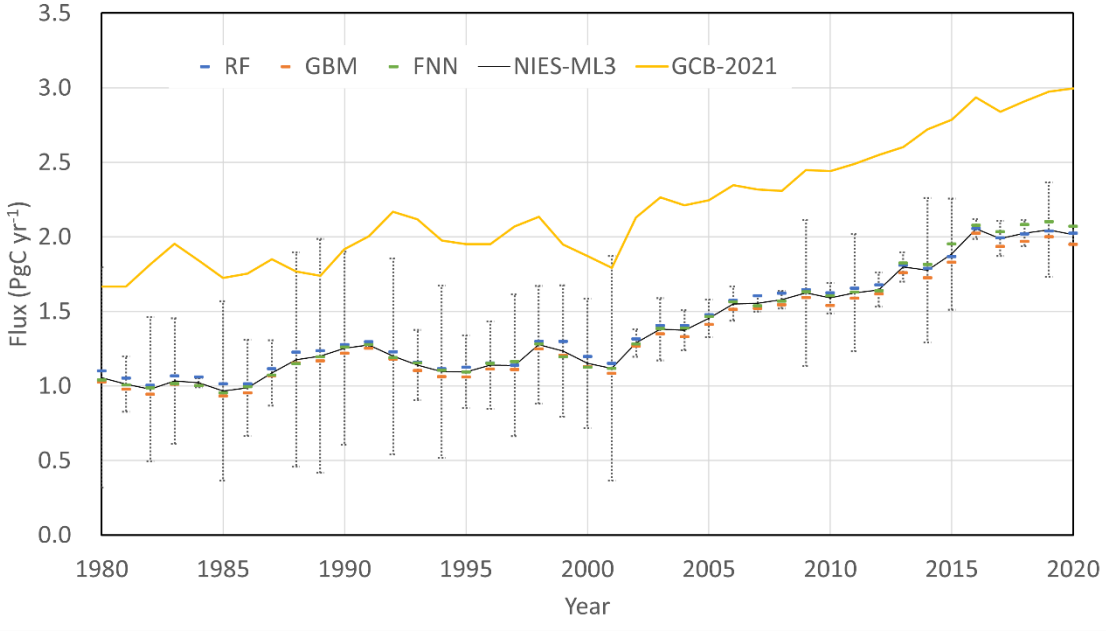

https://doi.org/10.5194/essd-2022-71
Preprint. Discussion started: 11 March 2022

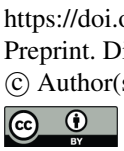

Open Access Earth System Science Data Discussions

Figure 3: Annual air-sea fluxes. The grey line (NIES-ML3) represents the mean fluxes of the random forest (blue), gradient boost machine (orange), and feedforward neural network (green) models. The error bars are uncertainty estimates using the mean biases of the three models in Table 2. The yellow line shows the mean fluxes of the biogeochemical models in Global Carbon Budget 2021. The difference between NIES-ML3 and GBC-2021 can be attributed to riverine input and coastal areas not included in NIES-ML3.

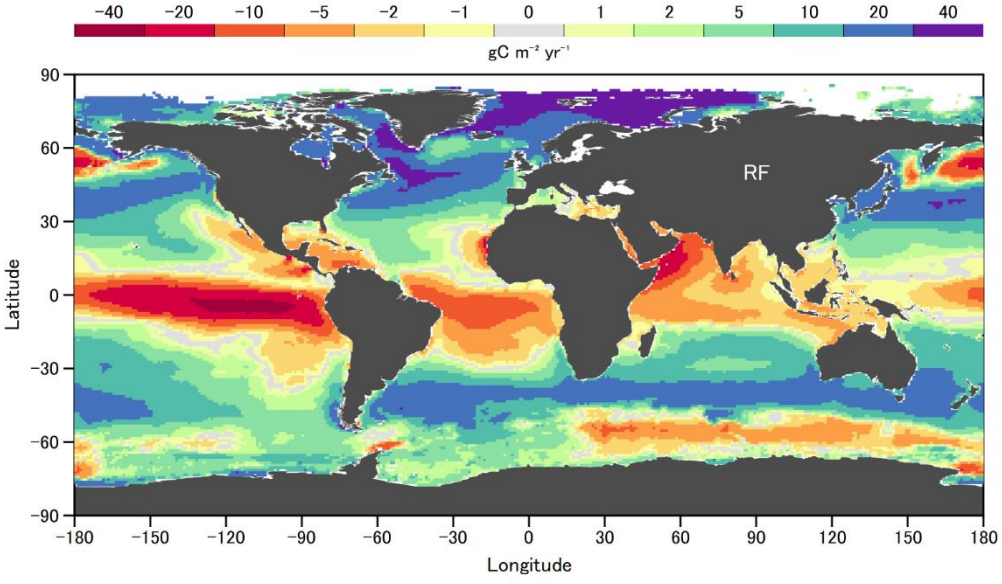

(a)

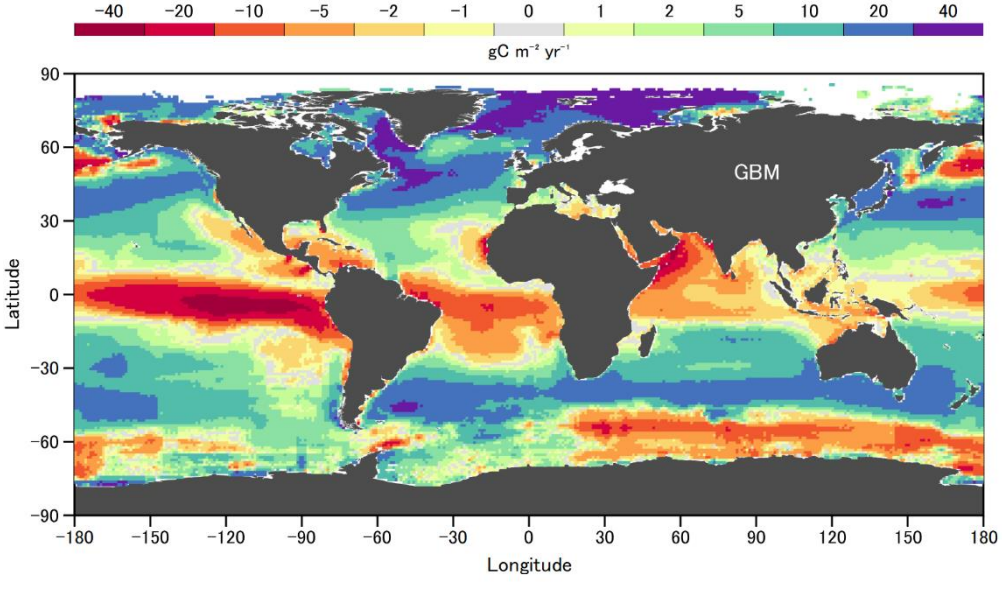

https://doi.org/10.5194/essd-2022-71
Preprint. Discussion started: 11 March 2022

Open Access Earth System Science Data Discussions

(b)

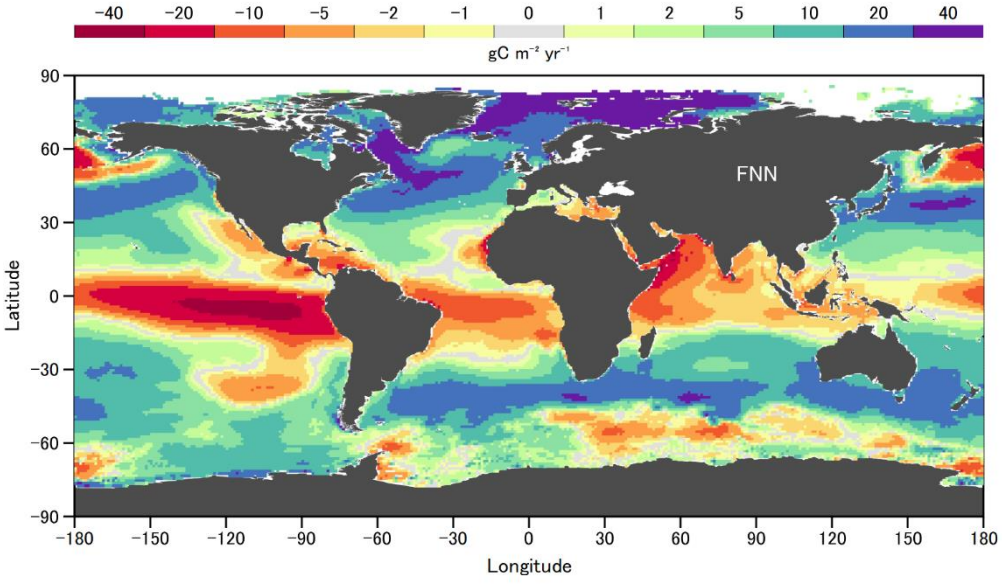

(c)

540

Figure 4: Distribution of the mean annual air-sea flux in 1980-2020. The patterns agree well with those in GCB-2021. Large sinks are located above 30°N and in the 30°S-60°S zone.

https://doi.org/10.5194/essd-2022-71
Preprint. Discussion started: 11 March 2022

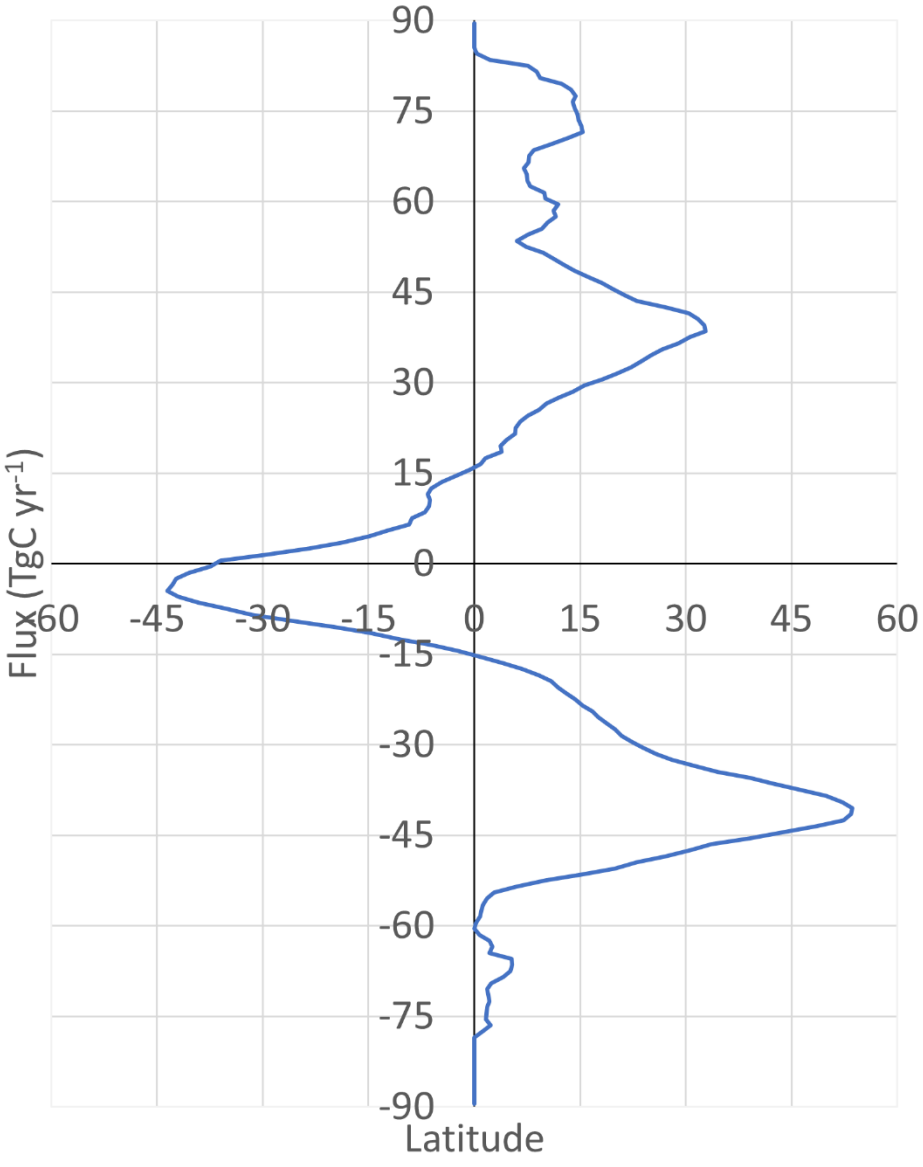

545 **Figure 5: Latitudinal profile of air-sea fluxes. The tropical areas were the net emitter and the oceans in mid latitude played as important sinks.**

https://doi.org/10.5194/essd-2022-71
Preprint. Discussion started: 11 March 2022

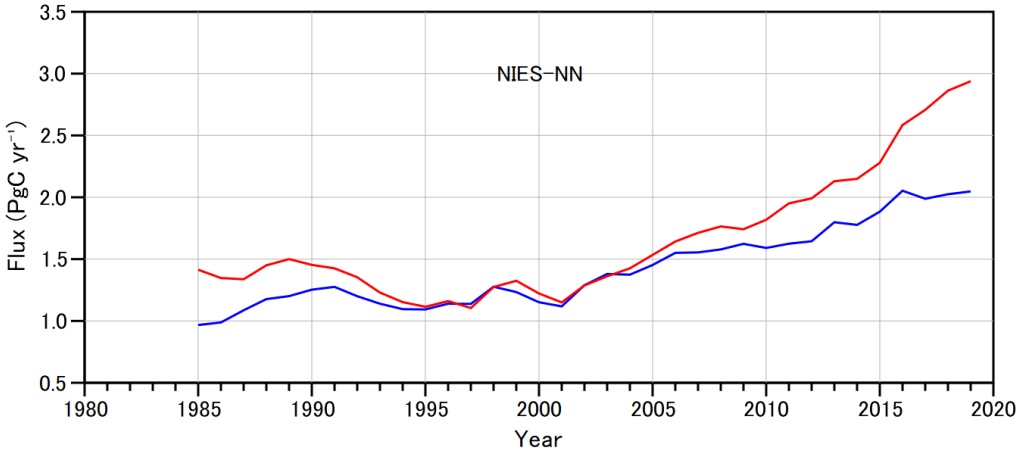

(a)

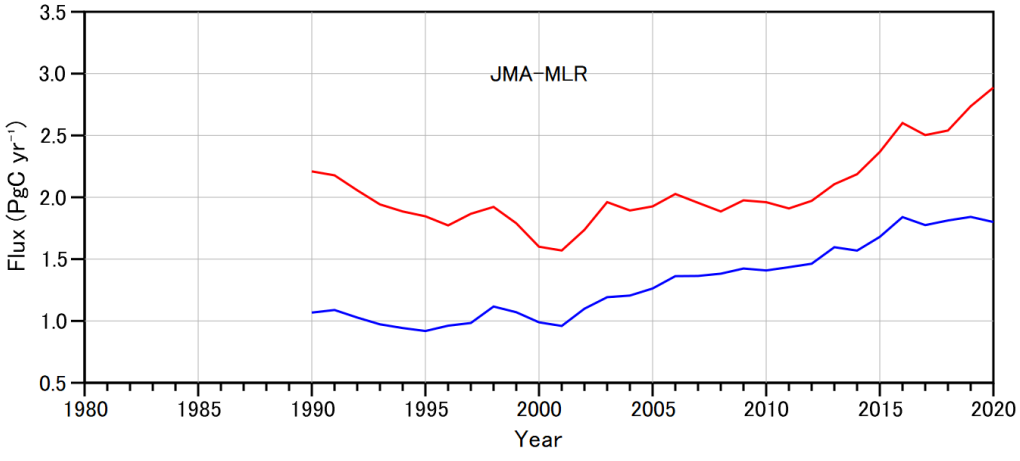

(b)

https://doi.org/10.5194/essd-2022-71
Preprint. Discussion started: 11 March 2022

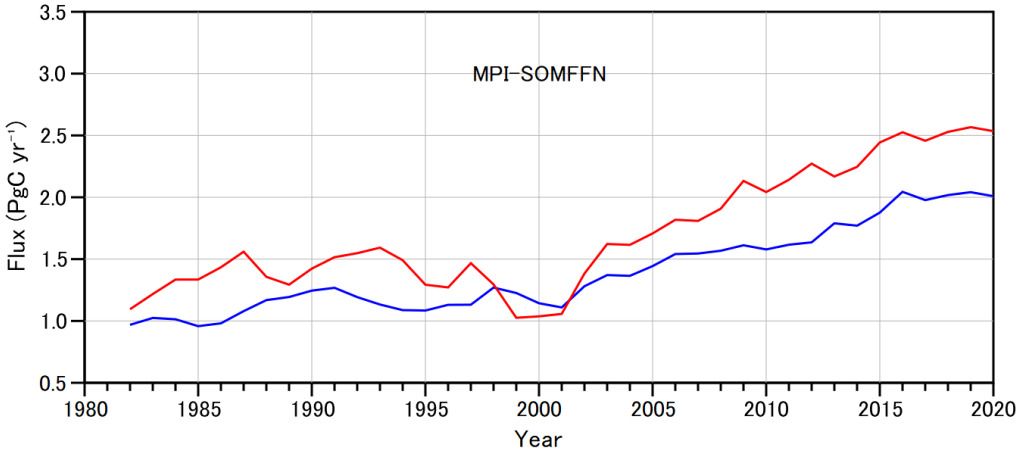

(c)

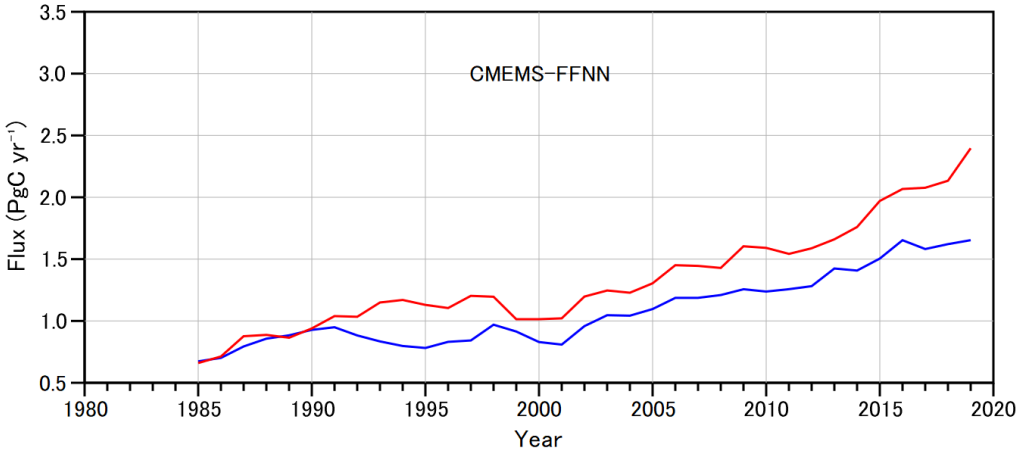

555 (d)

https://doi.org/10.5194/essd-2022-71
Preprint. Discussion started: 11 March 2022

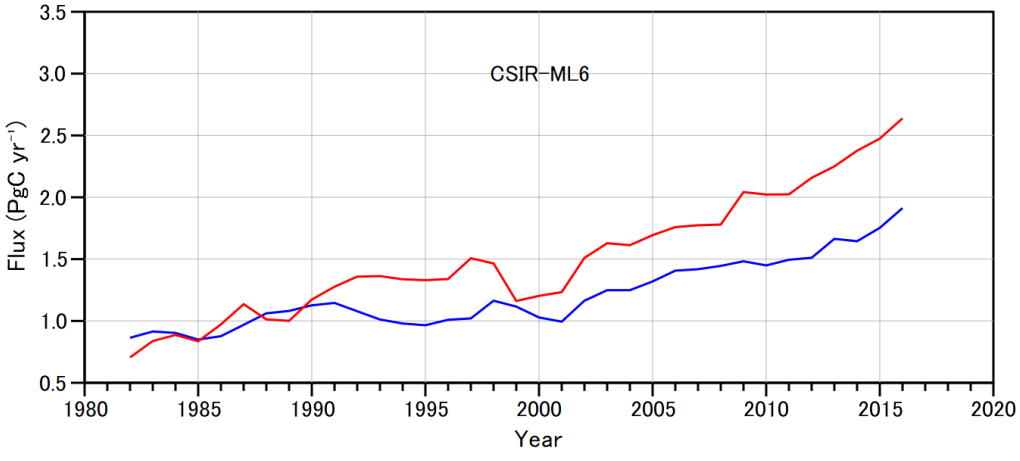

(e)

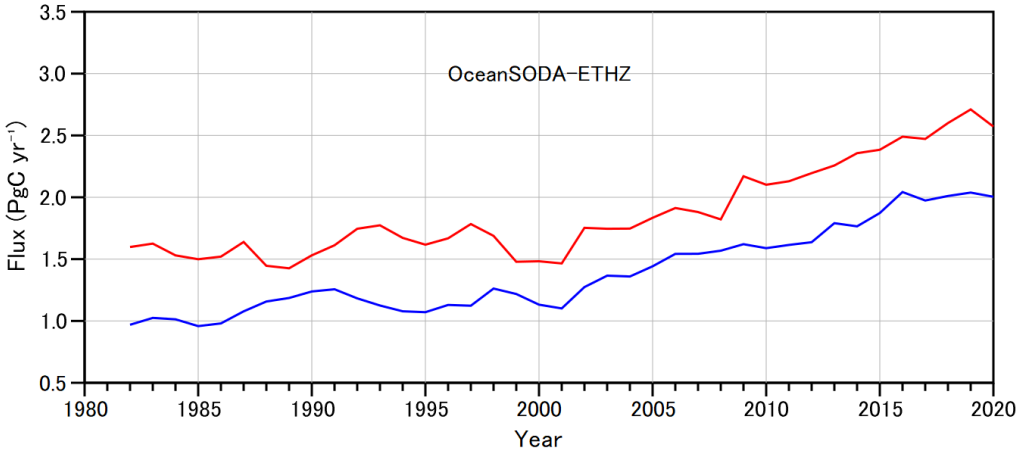

(f)

Figure 6: Comparisons with products included in GSB-2021. NIES-ML3 and the product under comparison are present by blue and red lines respectively. The comparisons are relative because of different spatial coverage and different parameters and wind products used for flux calculation. Only those grids where both products have data were counted to calculate the global sum.